GA–A27948

FIRST DIRECT EVIDENCE OF TURBULENCE-DRIVEN ION FLOW TRIGGERING THE L- TO H-MODE TRANSITION

By
L. SCHMITZ, B.A. GRIERSON, L. ZENG, J.A. BOEDO, T.L. RHODES, Z. YAN, G.R. McKEE, P. GOHIL, D. ELDON, L. BARDOCZI, C. CHRYSTAL, P.H. DIAMOND, W.A. PEEBLES, G.R. TYNAN, R.J. GROEBNER, K.H. BURRELL, C.C. PETTY, E.J. DOYLE and G. WANG

SEPTEMBER 2014

GENERAL ATOMICS

DISCLAIMER

GA–A27948

FIRST DIRECT EVIDENCE OF TURBULENCE-DRIVEN ION FLOW TRIGGERING THE L- TO H-MODE TRANSITION

By
L. SCHMITZ,* B.A. GRIERSON,† L. ZENG,* J.A. BOEDO,‡ T.L. RHODES,* Z. YAN,¶ G.R. McKEE,¶ P. GOHIL, D. ELDON,‡ L. BARDOCZI,* C. CHRYSTAL,‡ P.H. DIAMOND,‡ W.A. PEEBLES,* G.R. TYNAN,‡ R.J. GROEBNER, K.H. BURRELL, C.C. PETTY, E.J. DOYLE* and G. WANG*

This is a preprint of a paper to be presented at the Twenty-Fifth IAEA Fusion Energy Conf., October 13-18, 2014 in Saint Petersburg, Russia and published in the *Proceedings*.

*University of California Los Angeles, Los Angeles, California.
†Princeton Plasma Physics Laboratory, Princeton, New Jersey.
‡University of California San Diego, La Jolla, California.
¶University of Wisconsin-Madison, Madison, Wisconsin.

Work supported by
the U.S. Department of Energy
under DE-FG02-08ER54984, DE-AC02-09CH11466,
DE-FG02-07ER54917, DE-FG02-89ER53296, and DE-FG02-08ER54999

GENERAL ATOMICS PROJECT 30200
SEPTEMBER 2014

GENERAL ATOMICS

First Direct Evidence of Turbulence-Driven Ion Flow Triggering the L- to H-Mode Transition

EX/11-4

L. Schmitz,[1] B.A. Grierson,[2] L. Zeng,[1] J.A. Boedo,[3] T.L. Rhodes,[1] Z. Yan,[4] G.R. McKee,[4] P. Gohil,[5] D. Eldon,[3] L. Bardoczi,[1] C. Chrystal,[3] P.H. Diamond,[3] W.A. Peebles,[1] G.R. Tynan,[3] R.J. Groebner,[5] K.H. Burrell,[5] C.C. Petty,[5] E.J. Doyle,[1] and G. Wang[1]

[1]University of California Los Angeles, PO Box 957099, Los Angeles, CA 90095-7099, USA
[2]Princeton Plasma Physics Laboratory, PO Box 451, Princeton, NJ 08543-0451, USA
[3]University of California San Diego, 9500 Gilman Dr., La Jolla, CA 92093-0417, USA
[4]University of Wisconsin-Madison, 1500 Engineering Dr., Madison, WI 53706, USA
[5]General Atomics, PO Box 85608, San Diego, CA 92186-5608, USA
email: lschmitz@ucla.edu

Abstract Simultaneous measurements of main ion flow, $\boldsymbol{E}\times\boldsymbol{B}$ flow, and turbulence level $\tilde{n}/n$ inside the separatrix (LCFS) show for the first time that the initial turbulence collapse preceding the L-H transition is due to turbulence-driven $\boldsymbol{E}\times\boldsymbol{B}$ flow and ion flow in the ion diamagnetic direction, *opposing* the pressure-gradient-driven equilibrium $\boldsymbol{E}\times\boldsymbol{B}$ flow in the L-mode phase. Low to high confinement (L-H) transitions characterized by limit cycle oscillations (LCO) allow probing the trigger dynamics and synergy of turbulence-driven meso-scale flows, and pressure-gradient driven flows with high spatio-temporal resolution. A density scan indicates that the seed flow shear at the L-mode to LCO transition is lowest near the power threshold minimum. Causality of shear-flow generation has been established: early during LCO, the $\boldsymbol{E}\times\boldsymbol{B}$ shearing rate leads the ion pressure gradient response; as the LCO evolves, the edge pressure gradient and ion diamagnetic flow increase substantially, and the shearing rate lags the ion pressure gradient. Pressure-gradient-driven shear flow then becomes sufficiently large to secure the final LCO-H-mode transition. A two-predator, one-prey model, retaining arbitrary polarity of turbulence-driven flow, captures essential aspects of the transition dynamics, including the magnitude and direction of the driven poloidal main ion flow.

1. Introduction

Developing a physics-based model of the L-H transition is critical for confidently extrapolating the auxiliary heating requirements for ITER from the existing empirical L-H transition power threshold scaling. For the first time, it is shown here that the initial (transient) turbulence collapse preceding the L-H transition is caused by turbulence-generated poloidal ion flow and $\boldsymbol{E}\times\boldsymbol{B}$ flow *opposing* the equilibrium (L-mode) edge plasma $\boldsymbol{E}\times\boldsymbol{B}$ flow. *Subsequently,* the edge pressure gradient ∇P_i and the pressure-gradient-driven $\boldsymbol{E}\times\boldsymbol{B}$ flow shear increase periodically, eventually sustaining turbulence suppression and H-mode confinement.

Evidence from several recent experiments [1–7] has pointed towards a synergistic role of turbulence-driven flows [Zonal Flows (ZFs)] and pressure-gradient-driven flows in the trigger and evolution of the L-H transition. The Reynolds stress, and the nonlinear energy transfer between the turbulence spectrum and the turbulence-driven flow, have been evaluated recently for specific plasma parameters [8–10]. Near power threshold, the transition dynamics is substantially expanded/slowed via limit cycle oscillations (LCO) [4–7] between the turbulence amplitude and the fluid $\boldsymbol{E}\times\boldsymbol{B}$ velocity, allowing profile and flow measurements to be made with unprecedented spatial and temporal resolution. L-H transitions preceded by LCO have been obtained in DIII-D near marginal input power P_{th} ($0.75 \le P/P_{th} \le 2$) across a range of plasma currents ($0.6 \le I_p \le 1.5$ MA), edge safety factor ($3.8 \le q_{95} \le 8$), and plasma density ($1\text{x}10^{19}$ m^{-3} $\le \langle n \rangle \le 5.5\text{x}10^{19}$ m^{-3}). In the experiments reported here we have measured evolution of the turbulence (density fluctuation level), the total $\boldsymbol{E}\times\boldsymbol{B}$ flow velocity, the ion pressure gradient, and the poloidal main ion mean flow, across the high and low density branch of the L-H transition power threshold scaling.

2. Experimental Evidence for Turbulence-Driven *E*×*B* and Ion Flow

Figure 1(a,b) show the time evolution of the density fluctuation level $\tilde{n}$, measured via Doppler backscattering (DBS) [11,12] at a normalized wave-number $k_\theta\rho_s$~0.5 (measured with a half-width wave-number resolution $\Delta k_\theta/k_\theta$~0.4), and the total ***E***×***B*** velocity determined from the Doppler shift of the backscattered signal, in a lower single null (LSN) diverted deuterium plasma (L-mode density $\langle n \rangle = 3\text{x}10^{19}$ m^{-3}, I_p = 0.75 MA, B~1.8 T). The data shown in Fig. 1(a-d) is obtained 3 cm above the tokamak midplane, outboard of the minimum in the radial electric field (in the outer ***E***×***B*** shear layer). The radius and poloidal wave-number probed by DBS are extracted via GENRAY ray tracing, using density radial profiles reconstructed with high time resolution (25 μs) from profile reflectometry. Figure 1(c) shows the $\mathbf{v}_i$×***B*** component of the ***E***×***B*** velocity, calculated from the main ion momentum balance equation $\mathbf{v}_{E\times B} = \left(Z_i e n_i B\right)\partial n_i T_i / \partial r + \left(\mathbf{v}_i \times \mathbf{B}\right)/B$ by subtracting the measured pressure gradient term from the total ***E***×***B*** velocity (where Z_i, n_i, T_i, and v_i are the main ion charge number, density, temperature and fluid velocity). ∇P_i is approximated using the electron density from profile reflectometry (as Z_{eff}~1.6 and $n_{iC} << n_i$) and the carbon ion temperature from charge exchange recombination (CER) (assuming $T_{iC} \sim T_i$). Fluctuation suppression is first observed in the outer shear layer at $t=t_0$ during a positive peak of the $\mathbf{v}_i$×***B*** term [Fig. 1(c)]. A local ***E***×***B*** flow reversal is also observed at this time [Fig. 1(d)], leading to concomitant large positive and negative shearing rates within a narrow (2 cm) radial region, characteristic of turbulence-driven (meso-scale) flows. Figure 1(e) shows that the (negative) shearing rate in the inner shear layer (inboard of the minimum) does not initially increase significantly as fluctuations are first suppressed, but starts oscillating at the LCO frequency and eventually becomes periodically more negative as the LCO evolves. Hence the outer shear layer is initially most significant for fluctuation suppression and initiating the LCO.

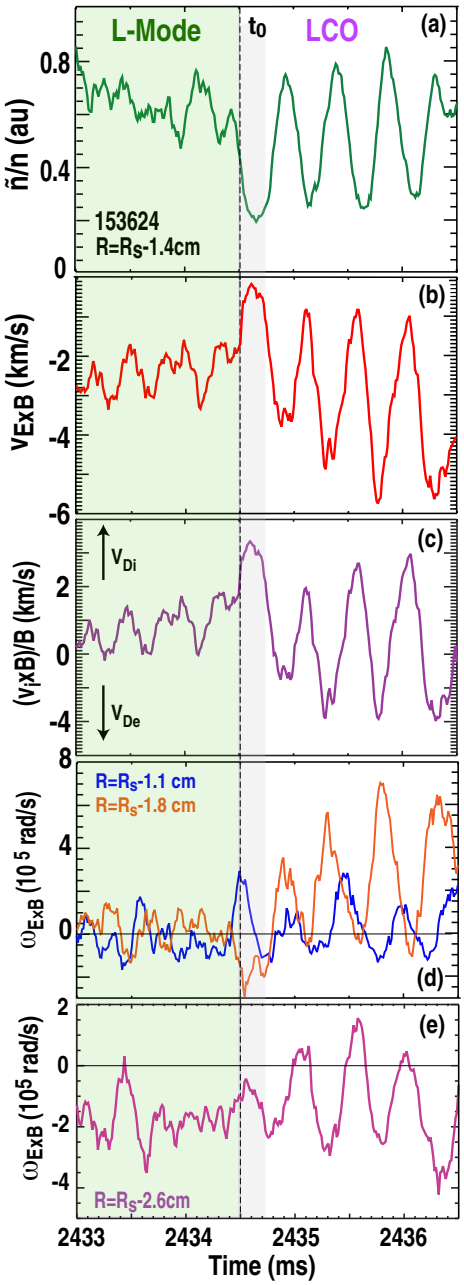

Fig. 1. Time evolution of (a) density fluctuation level; (b) ***E***×***B*** velocity; (c) main ion $\mathbf{v}$×***B*** contribution to the ***E***×***B*** velocity; (d) shearing rate ω_{ExB} at two radii inside the LCFS; (e) shearing rate in the inner shear layer. Time of initial turbulence suppression is indicated by a grey bar. R_s is the LCFS radius.

Evidence for a dipolar meso-scale ***E***×***B*** flow structure in the LCO edge electric field layer is presented in Fig. 2, which shows a contour plot of the radial electric field evolution across the L-mode LCO transition (obtained from the measured Doppler shift of the DBS signal), along with the density fluctuation level from DBS. In L-mode, the radial electric field exhibits a shallow well structure with ***E***×***B*** flow in the electron diamagnetic direction

[Fig. 2(a)], compensating the ion diamagnetic flow due to the edge ion pressure gradient. As the LCO is triggered, the electric field plot shows periodic positive (ion-diamagnetic direction) $\boldsymbol{E}\times\boldsymbol{B}$ flow near the LCFS. The negative (electron-diamagnetic) excursions of $v_{E\times B}$ in the center of the electric field well (around R~2.26 m) become progressively larger and are clearly phase-shifted with respect to the positive peaks at/outside the LCFS. Furthermore, in the inboard shear layer, around R~2.23 m, the positive (ion-diamagnetic direction) peaks are delayed with respect to the positive peaks at the LCFS/outer shear layer, consistent with radial inward propagation of the flow structure [6]. The observed radial flow structure is also qualitatively consistent with the previously reported Reynolds stress measure-ments near the center of the electric field well [8], and the radial stress profile inferred from beam emission spectroscopy (BES) velocimetry measurements [13]. Comparing Figs 2(a) and 2(b), it is clearly seen that fluctuations are initially suppressed inside the LCFS concomitantly with a short (~200 μs) positive excursion of $v_{E\times B}$ [as shown in Fig. 1(b) and Fig. 2(a) after 2434.5 ms as a green-blue feature spanning the outboard and inboard shear layers]. The positive flow extends across the center of the electric field well as fluctuations are suppressed, counteracting the L-mode $\boldsymbol{E}\times\boldsymbol{B}$ flow, and leading to a transient shear reversal.

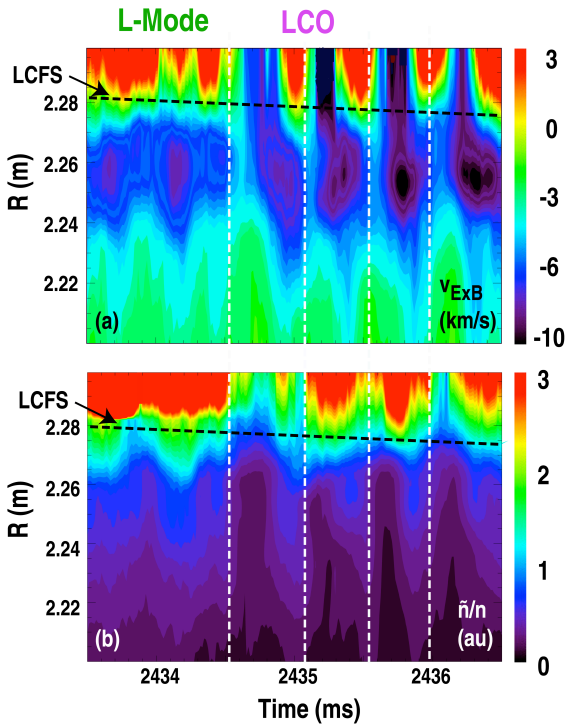

Fig. 2. (a) Contour plot of $\boldsymbol{E}\times\boldsymbol{B}$ velocity across the L-mode – LCO transition; (b) contour plot of density fluctuation level. The LCFS position is indicated. Start of turbulence suppression in each LCO cycle is indicated via white dashed lines.

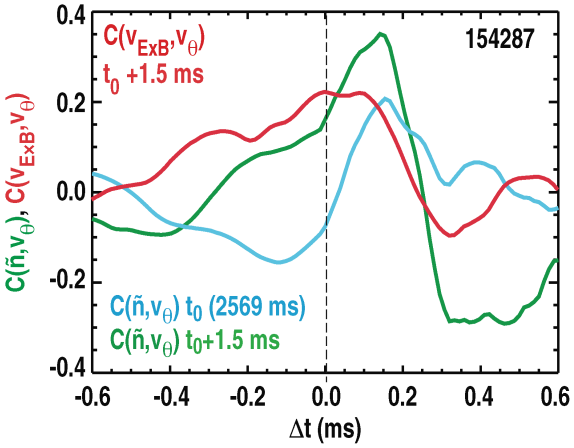

Fig. 3. Cross correlation coefficient of density fluctuation envelope $\tilde{n}$ and poloidal main ion flow velocity $v_{i\theta}$, at the L-LCO transition and 1.5 ms into the LCO phase. The cross correlation of the total $\boldsymbol{E}\times\boldsymbol{B}$ velocity with $v_{i\theta}$, 1.5 ms into the LCO phase, is also shown.

We show now that the observed positive flow transients are consistent with turbulence-driven poloidal ion flow and $\boldsymbol{E}\times\boldsymbol{B}$ flow, and inconsistent with turbulence suppression via diamagnetic (profile) shear in the early LCO phase. The cross-correlations between turbulence envelope, main ion flow, and pressure-gradient driven flow, and their detailed spatio-temporal evolution, have been measured in a helium plasma with dominant electron cyclotron heating (ECH) ($\langle n\rangle \sim 3.5\text{x}10^{19}$ m^{-3}, $I_p \sim 0.8$ MA, B=1.8 T). Figure 3 shows that the main ion poloidal mean flow $v_{i\theta}$ (obtained via main ion CER) lags $\tilde{n}$ after the L-mode-LCO transition and is nearly in phase with $v_{E\times B}$. Both results are consistent with turbulence-driven poloidal flow/ZF dominating $v_{E\times B}$ early during the LCO phase. Weak anti-correlation of $\tilde{n}$, and $v_{E\times B}$ with the toroidal ion flow is found in the early LCO, and the measured modulation of the toroidal flow velocity is a fraction (~15%-

30%) of the co-current toroidal velocity resulting from co-neutral beam injection (NBI) (which reaches ~35 km/s near the outboard LCFS as measured here via main ion (CER). Together with the results presented below in Fig. 5, this indicates that the poloidal velocity modulation is dominant early during the LCO and that the toroidal ion velocity modulation in the LCO is a fraction of the mean toroidal velocity resulting from the co-NBI beam torque.

3. Causality of Shear-Flow Generation

The causality of shear flow generation has been investigated via correlation analysis of the $\boldsymbol{E}\times\boldsymbol{B}$ flow-shearing rate and the ion pressure gradient/diamagnetic flow. Figure 4(a) shows that the total $\boldsymbol{E}\times\boldsymbol{B}$ shearing rate $\omega_{\mathbf{E}\times\mathbf{B}}$ leads the ion pressure gradient $-\nabla P_i$ early in the LCO ($t_o + 0.7$ ms), establishing clearly that the $\boldsymbol{E}\times\boldsymbol{B}$ flow shear modulation is not caused by $-\nabla P_i$ changes, but that the v_θ component is dominant. Later in the LCO ($t_o + 5.2$ ms), and closer to the final H-mode transition ($t_H = t_0$+13.5 ms), the periodic reduction in edge turbulence and edge transport enables a gradual increase (and periodic modulation) of the edge pressure gradient and the ion diamagnetic flow shear becomes dominant such that $\omega_{\mathbf{E}\times\mathbf{B}}$ then lags $-\nabla P_i$. In Fig. 4(b) the time evolution of the correlation delay between the shearing rate and the ion pressure gradient is shown. The correlation delay becomes negative ~3 ms after the LCO starts, indicating that the profile shear becomes dominant fairly early in this case.

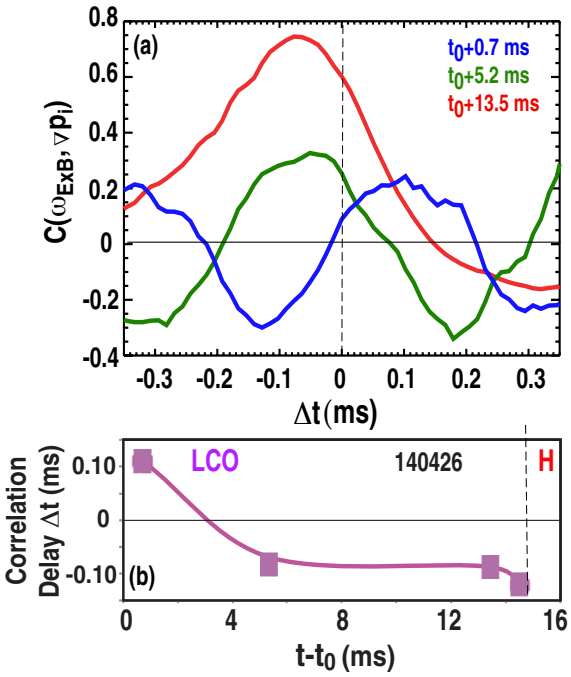

Fig. 4. (a) Cross-correlation coefficient between the $\boldsymbol{E}\times\boldsymbol{B}$ shearing rate $w_{\mathbf{ExB}}$ and the ion pressure gradient; shown are data for three times after the L-mode - LCO transition; (b) measured correlation delay vs elapsed time after LCO start.

Figure 5(a-c) show the time evolution of the density gradient (used here as proxy for the ion pressure gradient), the $\boldsymbol{E}\times\boldsymbol{B}$ flow and the density fluctuation level. It has been confirmed that the ion pressure gradient oscillations are in phase with the density gradient oscillations [13]. An expanded view [Fig. 5(d,e)] shows that $-\nabla P_i$ increases periodically, generating strong negative $\boldsymbol{E}\times\boldsymbol{B}$ flow (blue bar). The data suggest that later in the LCO phase, the turbulence growth rate (and $\tilde{n}$) increase due to the increasing $-\nabla P_i$ within each cycle, in turn driving radial transport and reducing $-\nabla P_i$. The turbulence then collapses due to depletion of turbulence energy [10]. Reduced radial transport then allows $-\nabla P_i$ to rise again, transiently maintaining fluctuation suppression via profile shear. During the final phase of the LCO the pressure gradient (diamagnetic flow) dominates the mean flow $\boldsymbol{E}\times\boldsymbol{B}$ shearing rate, which becomes sufficiently large to sustain fluctuation suppression and secure the LCO-H-mode transition.

A heuristic dynamical model has been used to describe the L-LCO-H-mode transition, using the predator-prey Eqns (1) and (2) for the evolution of $\tilde{n}$ and the turbulence-driven flow v_{ZF} [14,15] along with an equation describing diamagnetic flow ($v_{\nabla p}$) evolution (3), and an equation for the meann poloidal ion flow (4). This model is based on earlier theoretical work describing two-predator flow-turbulence interactions at the L-H transition [15,16]. In contrast to previous work, however, opposite polarity of ∇P_i –driven and fluctuation-driven $\boldsymbol{E}\times\boldsymbol{B}$/poloidal ion flow is retained here:

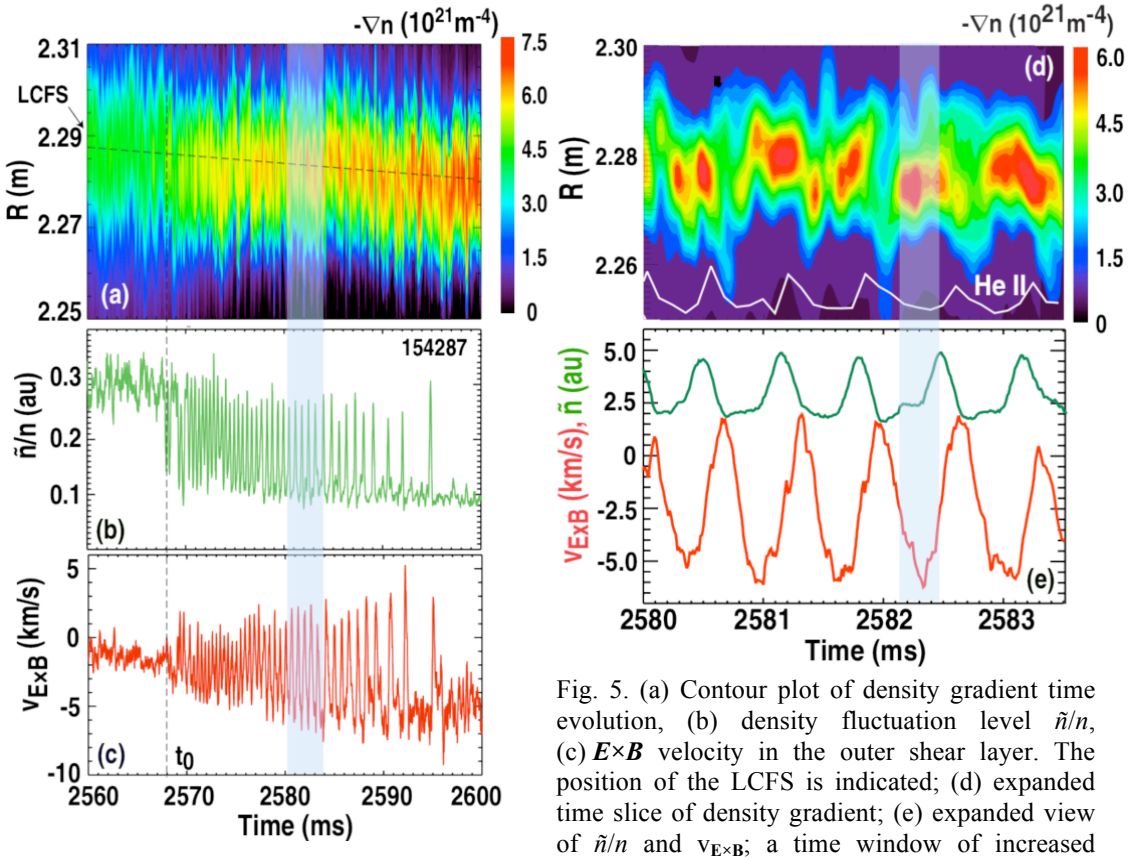

Fig. 5. (a) Contour plot of density gradient time evolution, (b) density fluctuation level $\tilde{n}/n$, (c) $\boldsymbol{E}\times\boldsymbol{B}$ velocity in the outer shear layer. The position of the LCFS is indicated; (d) expanded time slice of density gradient; (e) expanded view of $\tilde{n}/n$ and $v_{\mathbf{E}\times\mathbf{B}}$; a time window of increased density gradient is indicated.

$$\partial\tilde{n}/\partial t = \boldsymbol{\gamma}\tilde{n} - c_1 v_{ZF}\tilde{n} - c_2 v_{\nabla P} - c_3\tilde{n}^2 \quad (1)$$

$$\partial v_{ZF}/\partial t = c_4\tilde{n}^2 v_{ZF} - \boldsymbol{\gamma}_{ZF} v_{ZF} \quad (2)$$

$$-\partial v_{\nabla P}/\partial t = Q + c_5\tilde{n}^2 v_{\nabla P} + c_6 v_{\nabla P} \quad (3)$$

$$\partial v_{i\boldsymbol{\theta}}/\partial t = c_7\tilde{n}^2 - c_8 v_{i\boldsymbol{\theta}} - c_9 v_{\nabla P} \quad . \quad (4)$$

Here, Q is the (slowly increasing) radial heat flux driving the system, $\tilde{n}$ is the turbulence amplitude, and the constants c_1-c_3 describe, in order, turbulence depletion via turbulence-driven mesoscale shear flow, turbulence depletion via diamagnetically driven $\boldsymbol{E}\times\boldsymbol{B}$ shear flow, and the nonlinear turbulence saturation rate. $c_4\tilde{n}^2$ and γ_{ZF} describe the turbulent flow drive via the Reynolds stress radial gradient, and the Zonal Flow damping rate; $c_5\tilde{n}^2$ and c_6 describe the turbulent and neoclassical radial diffusion rates; and $c_7\tilde{n}^2$, c_8, and c_9 describe, in order, poloidal mean ion flow drive via the Reynolds stress, and neoclassical poloidal flow damping and gradient drive [4]. Toroidal flow is neglected here for simplicity. The initial modeling has been carried out using 0D equations, although a more advanced 1D model has also been developed and is needed in order to address the spatial evolution of the edge flow layer and the radial flow reversal described earlier. 1D modeling results will be discussed in a separate paper. Typical 0D modeling results applicable to the radial region at or just inside the LCFS are presented in Fig. 6 The LCO is triggered via an increase in the turbulence level $\tilde{n}$ (green) that drives concomitant meso-scale flow v_{ZF} [Fig. 6(b)] and mean poloidal ion flow $v_{i\theta}$ [Fig. 6(a)] in the positive (ion-diamagnetic) direction. In practice, the LCO can be triggered via an increase in turbulence amplitude leading to an increase in the energy transfer

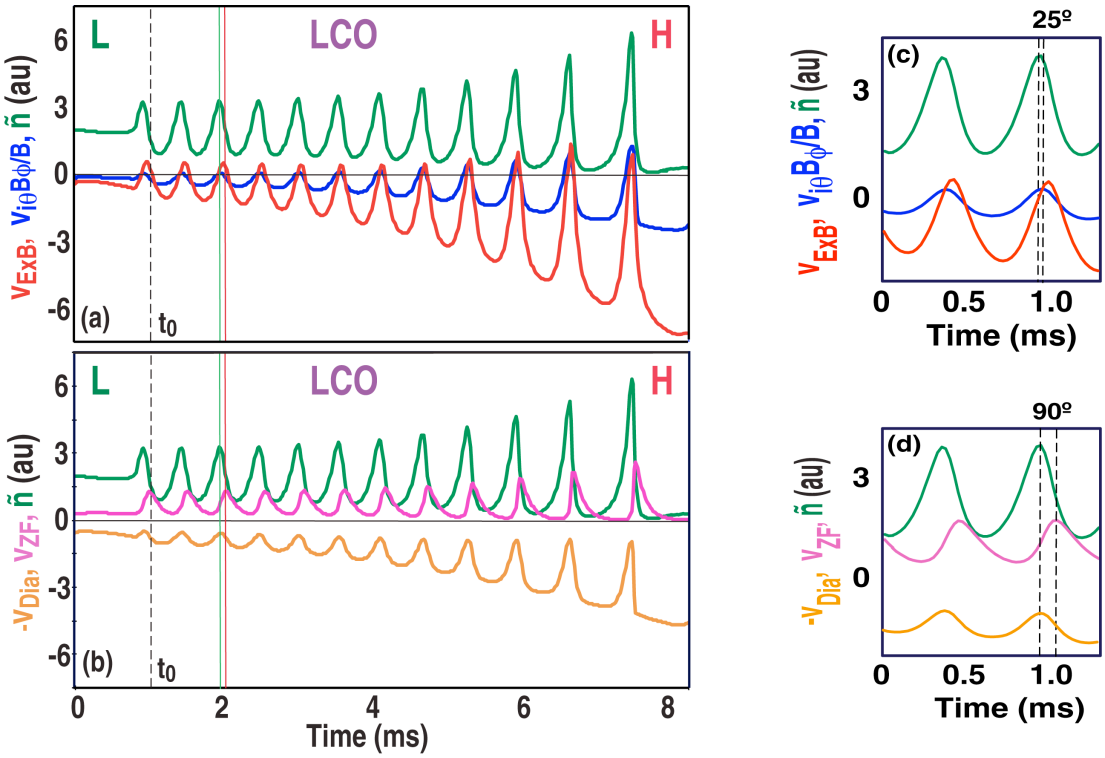

Fig. 6. 0D predator-prey modeling results: (a) Time evolution of the turbulence level $\tilde{n}$, the $\boldsymbol{E}\times\boldsymbol{B}$ velocity component associated with the mean poloidal ion flow $v_{i\theta}B_\phi/B$, and the total $\boldsymbol{E}\times\boldsymbol{B}$ velocity, across the L-mode-LCO-H-mode transition, (b) turbulence level $\tilde{n}$, turbulence-driven flow v_{ZF}, and diamagnetic component of the $\boldsymbol{E}\times\boldsymbol{B}$ velocity; (c) expanded view and phase delay of turbulence-driven flow, and total $\boldsymbol{E}\times\boldsymbol{B}$ flow with respect to the turbulence amplitude; (d) phase delay of mean poloidal ion flow and diamagnetic flow with respect to $\tilde{n}$.

rate from the turbulence spectrum into the low-frequency flow [8–10]. An increase in turbulence level can occur for example due to a step in auxiliary heating power, a radial turbulence avalanche event, an internal sawtooth crash and concomitant radial heat pulse. The trigger criterion for the LCO is that the turbulent energy transfer rate via the Reynolds stress exceeds the ambient turbulence decorrelation rate and the low frequency poloidal flow-damping rate, which will then cause the turbulence amplitude to collapse and the ZF and v_θ to increase markedly.

The 0D modeling results shown here are in agreement with and illustrate several important experimental observations. (i) The initial turbulence quench occurs during a positive $v_{i\theta}$ and $v_{\boldsymbol{E}\times\boldsymbol{B}}$ transient; the poloidal ion flow shows a small phase lag with respect to $\tilde{n}$ (~25º in the modeling results, similar to the experimental observation (Fig. 3). (ii) The driven mean ion poloidal flow excursions (blue) oppose the diamagnetic component of the $\boldsymbol{E}\times\boldsymbol{B}$ velocity, v_{dia}. (iii) Positive $v_{i\theta}$ (blue) excursions lag $\tilde{n}$ with a ~25º similar to that observed experimentally (Fig. 3); the phase delay of the positive Zonal $\boldsymbol{E}\times\boldsymbol{B}$ flow component with respect to $\tilde{n}$, is 90º in the LCO as expected for a predator-prey relationship and observed experimentally in Fig. 1(a,b)]. (iv) The LCO decreases in frequency (and eventually ceases) due to increasing diamagnetic flow (orange), and pressure-gradient driven shear $-\partial/\partial r(v_{dia})$ and concomitantly increasing delay of the turbulence recovery; increasing pressure-gradient-driven shear is clearly observed to secure the final transition to H-mode in the modeling results. (v) Pressure gradient oscillations during the LCO are out of phase with $\tilde{n}$ [Fig. 6(d)], indicating that the pressure gradient increases after turbulence suppression in each LCO cycle, again in agreement with experimental observations.

4. Role of Seed Flow Shear

The ultimate goal of a detailed physics-based L-H transition model is to interpret the observed power threshold scaling and allow threshold predictions for future burning plasmas. The energy transfer from the ambient L-mode turbulence into directional mesoscale flows is the important quantity that couples the LCO trigger dynamics to the power threshold. This energy transfer has been described by a rate equation for the (low frequency) flow energy W (where $\langle \tilde{v}_\theta \tilde{v}_r \rangle$ is the Reynolds stress and v_θ is the poloidal ion flow [10]):

$$\frac{\partial W}{\partial t} = \langle \tilde{v}_\theta \tilde{v}_r \rangle \frac{\partial v_\theta}{\partial r} - \gamma_{ZF} W - \frac{\partial}{\partial r} \langle \tilde{v}_\theta \tilde{v}_r \rangle v_\theta \quad . \tag{5}$$

If the flow damping and the third term on the right hand side (describing radial spreading of the low frequency flow energy) are neglected, the turbulence-flow energy transfer is proportional to the Reynolds stress and the radial shear of the poloidal ion velocity. A density dependence of the turbulent energy transfer could result from a density dependence of the Reynolds stress, or the (seed) flow-shearing rate. In addition to macroscopic turbulence levels, we are examining the maximum $\boldsymbol{E}\times\boldsymbol{B}$ flow-shearing rate and the flow shearing rates due to the diamagnetic and the $\mathbf{v}\times\boldsymbol{B}$ term in the radial ion momentum balance in the outer shear layer [the latter evaluated from $\omega_{\mathbf{E}\times\mathbf{B}}$ via subtracting the diamagnetic (profile) shear]. Preliminary results for the different contributions to the L-mode shearing rate are shown in Fig. 7, using a ~10 ms time average just before the L-mode-LCO transition. Data for D,H, and He plasmas are included. Both the (total) $\boldsymbol{E}\times\boldsymbol{B}$ shearing rate and its $\mathbf{v}\times\boldsymbol{B}$ component are seen to increase towards low and high plasma densities [Fig. 7(a)], with minimum values close to the density where the minimum transition threshold power is observed ($\langle n \rangle_{min}$ ~ 2-3x10^{19} m^{-3}). In contrast, the diamagnetic L-mode shearing rate peaks near $\langle n \rangle_{min}$. If the flux-surface averaged toroidal velocity shear [17] is small, the $\mathbf{v}\times\boldsymbol{B}$ shearing rate reflects primarily the poloidal velocity shear. The density dependence of the diamagnetic shear is less pronounced [Fig. 7(b)]; no or only a weak density dependence of the latter had also been observed previously in the ASDEX-U and JET tokamaks [18,19]. Hence the data indicates that the poloidal velocity seed flow shear may scale similarly with density as the L-H transition power threshold, and that enhanced poloidal velocity seed flow shear may be required to initiate the transition at low density.

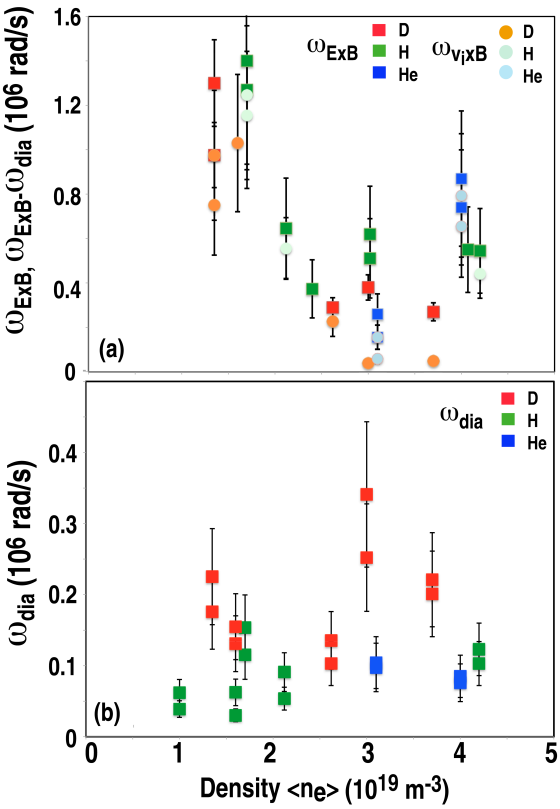

Fig. 7 (a) L-mode $\boldsymbol{E}\times\boldsymbol{B}$ flow shearing rates and $\omega_{\mathbf{E}\times\mathbf{B}}$-$\omega_{dia}$ just before the L-mode-LCO transition; ~1 cm inside the LCFS, vs line-averaged plasma density; shown are data for D, H, and He plasmas; (b) diamagnetic (profile) shearing rates.

5. Summary

We provide direct evidence of the role of turbulence-driven ZF/main ion poloidal flow in triggering the LCO, and initiating the transition to H-mode confinement. The synergy of turbulence-driven and pressure-gradient-driven flows in accessing H-mode confinement has been confirmed, with pressure-gradient driven flows dominating late in the LCO phase and securing the final LCO-H-mode transition. Causality of turbulence-driven flow in shear flow generation at the L-mode-LCO transition has been established. The observation of a turbulence-driven poloidal main ion flow in the ion diamagnetic direction also explains the direction of the $\tilde{n}$, v_{ExB} limit cycle observed in the outboard shear layer in DIII-D [13] and recently in JFT-2M [20] and in HL-2A under certain conditions [21], which is consistent only with positive (ion diamagnetic direction) flow drive. It should be noted that positive flow transients preceding fluctuation suppression have also been observed in regular "fast" L-H transitions in DIII-D using the same diagnostic tools. These results confirm the role of turbulence-driven flow in initiating the L-H transition as observed in regular (fast) L-H transitions in DIII-D [9] and C-Mod [10]), and preceding the subsequent pressure gradient/diamagnetic shear flow evolution leading to H-mode confinement [10]. A predator-prey model incorporating turbulence-driven flow, pressure gradient evolution and diamagnetic flow shear as well as mean ion poloidal flow evolution, describes qualitatively the essential experimental observations, including the phasing of turbulence amplitude, main ion poloidal flow, the pressure gradient oscillation and the total $\boldsymbol{E}\times\boldsymbol{B}$ flow.

To investigate the role of seed flow shear, the scaling of the $\boldsymbol{E}\times\boldsymbol{B}$, diamagnetic, and poloidal flow shearing rates with density have been measured. Preliminary results indicate that the L-mode poloidal seed flow shear just before the L-mode-LCO transition varies with density in a similar fashion than the L-H transition threshold power, and may play a t role in the observed density scaling of the L-H power threshold.

This material is based upon work supported by the U.S. Department of Energy, Office of Science, Office of Fusion Energy Sciences, using the DIII-D National Fusion Facility, a DOE Office of Science user facility, under Awards DE-FG02-08ER54984, DE-AC02-09CH11466, DE-FG02-07ER54917, DE-FG02-89ER53296, DE-FG02-08ER54999, and DE-FC02-04ER54698.

References

[1] G.R. McKee, et al., Nucl. Fusion **49**, 115016 (2009).
[2] S.J. Zweben, R.J.Maqueda, R. Hager, et al., Phys. Plasmas **17**, 102502 (2010).
[3] G.D. Conway, C. Angioni, F. Ryter, et al., Phys. Rev. Lett. **106**, 065001 (2011).
[4] G.S. Xu, et al., Phys. Rev. Lett. **107**, 125001 (2011).
[5] T. Estrada, C. Hidalgo, T. Happel, et al., Phys. Rev. Lett. **107**, 245004 (2011).
[6] L. Schmitz, L. Zeng, T.L. Rhodes, et al., Phys. Rev. Lett. **108**, 155002-5 (2012).
[7] J. Cheng, J.Q. Dong, K. Itoh, et al., Phys. Rev. Lett. **110**, 265002 (2013).
[8] G. Tynan, et al., Nucl. Fusion **53**, 073053 (2012).
[9] Z. Yan, G.R. McKee, R. Fonck, et al., Phys. Rev. Lett. **112**, 125002 (2014).
[10] I. Cziegler, G.R. Tynan, P.H. Diamond, et al., Plasma Phys. Control. Fusion **56**, 075013 (2014).
[11] W.A.Peebles, T.L. Rhodes, J.C. Hillesheim, et al., Rev. Sci. Instrum. **81**, 10D902 (2010).
[12] J.C. Hillesheim, et al., Rev. Sci. Instrum. **81**, 10D907 (2010).
[13] Z. Yan, G.R. McKee, private communication
[14] L. Schmitz et al., Nucl. Fusion **54**, 073012 (2014).
[15] E.J. Kim and P.H. Diamond, Phys. Rev. Lett. **90**, 185006 (2003).
[16] K. Miki and P.H. Diamond, Phys. Plasmas **19**, 092306 (2012).
[17] J. Boedo, E. Belli, E. Hollmann, et al., Phys. Plasmas **18**, 032510 (2011).
[18] P. Sauter, C. Puetterich, F. Ryter, et al., Nucl. Fusion **52**, 012001 (2012).
[19] C. Maggi, E. Dalabie, T.M. Biewer, et al. Nucl. Fusion **54**, 023007 (2014)
[20] T. Kobayashi, et al., Phys. Rev. Lett. **111**, 035002 (2013)